The Journal of Supercritical Fluids 149 (2019) 54–63

Contents lists available at ScienceDirect

The Journal of Supercritical Fluids

journal homepage: www.elsevier.com/locate/supflu

Heat treatment induced phase transformations in zirconia and yttria-stabilized zirconia monolithic aerogels

Jorge Torres-Rodríguez[a], József Kalmár[b,c,*], Melita Menelaou[a], Ladislav Čelko[a], Karel Dvořak[d], Jaroslav Cihlář[a], Jaroslav Cihlař Jr[a], Jozef Kaiser[a], Enikő Győri[b], Péter Veres[b], István Fábián[b,c], István Lázár[b]

[a] Central European Institute of Technology, Brno University of Technology, Purkyňova 123, 612 00 Brno, Czech Republic
[b] Department of Inorganic and Analytical Chemistry, University of Debrecen, Egyetem tér 1, Debrecen, H-4032 Hungary
[c] MTA-DE Redox and Homogeneous Catalytic Reaction Mechanisms Research Group, Egyetem tér 1, Debrecen, H-4032 Hungary
[d] AdMaS Center, Faculty of Civil Engineering, Brno University of Technology, Purkyňova 139, 612 00 Brno, Czech Republic

GRAPHICAL ABSTRACT

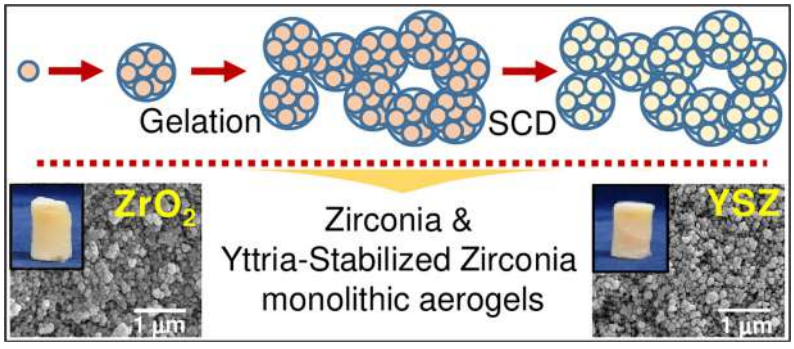

ARTICLE INFO

Keywords:
Aerogel
Zirconia
Yttria-stabilized zirconia
Heat treatment
Phase transformation

ABSTRACT

Monolithic, structurally stable zirconia (ZrO_2) aerogels can be used in high temperature applications and as medical implants. The macroscopic properties of these solids can be fine-tuned by the appropriate thermal treatment of the amorphous aerogels. Herein, we investigate the thermally induced phase transitions of ZrO_2 and yttria-stabilized zirconia (YSZ) monolithic aerogels. All aerogels were produced by an acid-catalyzed sol-gel technique and subsequent supercritical drying (SCD). A complete reaction mechanism is proposed for the formation of the wet gel network. Also, the phase transformations taking place during calcination were followed as function of temperature by *in-situ* X-ray diffraction measurements. Composition and size of the forming crystallites were calculated from the XRD data. Phase transition is controlled by the temperature-dependent growth of crystallite size during calcination up to 1200 °C. Both tetragonal and monoclinic zirconia form in pure ZrO_2 aerogels, and a single tetragonal phase forms in YSZ aerogels.

* Corresponding author at: Department of Inorganic and Analytical Chemistry, University of Debrecen, Egyetem tér 1, Debrecen, H-4032 Hungary.
E-mail address: kalmar.jozsef@science.unideb.hu (J. Kalmár).

https://doi.org/10.1016/j.supflu.2019.02.011
Received 14 November 2018; Received in revised form 31 January 2019; Accepted 11 February 2019
Available online 27 February 2019
0896-8446/

1. Introduction

Aerogels are highly porous materials, which are composed of interconnected nanoparticles in an open mesoporous 3D structure [1]. Generally, the formation of aerogels involves the formation of a colloidal suspension (sol), that is followed by the transition of the sol into a gel, and finally, the extraction of the solvent while keeping the solid backbone intact [2,3]. They are excellent candidates for thermal and acoustic insulation, radiation detectors, drug delivery systems and catalyst supports [4–6].

Zirconia (ZrO_2) is a high-temperature oxide which has excellent heat resistance, high toughness, abrasion resistance and chemical resistance. It has been studied for several applications in catalysis, in engineering as a structural material and as a semiconductor [7,8]. In order to improve the performance of ZrO_2-based materials, a high surface area and the phase stability of zirconia are desirable characteristics. Pure ZrO_2 is a polymorphic oxide that has three well-known thermodynamically stable crystalline phases: *i*) the monoclinic phase (*m*-ZrO_2) which is stable from room temperature to 1170 °C, *ii*) the tetragonal phase (*t*-ZrO_2) which is stable between 1170 and 2370 °C and *iii*) the cubic (*c*-ZrO_2) phase exists between 2370 and 2680 °C A metastable tetragonal zirconia is also known and can be stable below 650 °C [9]. The crystalline phase of zirconia affects its macroscopic structural and textural properties, such as the specific surface area, porosity, density and particle size. When zirconia is stabilized in the tetragonal phase, high strength, toughness and wear resistance rise. Several studies have indicated that pure *t*-ZrO_2 can be stabilized in the nanoscale at temperatures lower than 1170 °C under well-adjusted synthetic conditions [10–12]. The calcination temperature (from 400 to 700 °C) has a direct effect on the transformation of zirconia from *t*-ZrO_2 to *m*-ZrO_2, and that this transformation is accompanied by the growth of the crystallite size. In addition to the structural stability of zirconia, the textural properties, such as the surface area, are also affected by the synthetic methods [13–17]. In spite of the numerous efforts to produce zirconia aerogel monoliths, the resulting ceramics have poor thermal stability that renders them less attractive in high temperature applications.

Several chemical approaches are focused on the stabilization of *t*-ZrO_2. One approach is the doping of zirconia by di- or trivalent cations (M^{3+}, M^{2+}) with suitable ionic radii in order to replace the Zr^{4+} in the sublattice. The charge in these hybrids is balanced by the formation of oxygen vacancies. A representative example is the case of Y^{3+} ions, the use of which results in the stabilization of high-temperature zirconia phases at room temperature. Typically, 6–8 mol % of ZrO_2 is substituted by Y_2O_3, and the resulting hybrid is called yttria-stabilized zirconia (YSZ) [18–20]. Also, several attempts have been reported to enhance the crystallinity, as well as the mechanical properties of zirconia aerogels by hybridization with silica [21–23]. It is important to understand the role of critical variables affecting the stability of *t*-ZrO_2 in monolithic aerogels in order to fine tune the macroscopic characteristics [10,19,24].

In spite of the large variety of the above mentioned approaches, much less work has been devoted to investigate the intimate effect of heat treatment on amorphous ZrO_2 and YSZ aerogels. In this paper we report the synthesis of monolithic ZrO_2 and YSZ aerogels through a facile acid-catalyzed sol-gel method. We thoroughly investigate the effect of heat treatment on the crystallographic evolution and the phase stability of both systems starting from the as-prepared amorphous aerogels.

2. Experimental

2.1. Materials

All chemicals were purchased from Sigma-Aldrich and used as received. Zirconium(IV) propoxide ($Zr(OC_3H_7)_4$, 70 wt% in *n*-propanol), yttrium(III) nitrate hexahydrate ($Y(NO_3)_3{\cdot}6H_2O$), nitric acid (HNO_3, 70%), acetone and *n*-propanol (anhydrous) were used for the synthesis.

2.2. Synthesis of wet gels

ZrO_2 wet gels were prepared in the following 4 steps: *i*) a 1 M HNO_3 solution was prepared in n-propanol (catalyst solution); *ii*) in a separate beaker, 2.5 mL zirconium(IV) propoxide was mixed with 12.5 mL n-propanol and with 0.75 mL catalyst solution under continuous stirring (solution A); *iii*) a third solution was prepared from 0.75 mL distilled water and 12.5 mL *n*-propanol (solution B) and *iv*) solution B was slowly added to solution A and stirred vigorously with a magnetic stir bar for 5 min [25]. After these steps, the mixture was poured into cylindrical plastic molds, hermetically sealed and let to stand at room temperature for one day in order to form the wet ZrO_2 gel. The final molar ratio of Zr $(OC_3H_7)_4$, HNO_3 and H_2O were 1:2:3.

For the preparation of YSZ wet gels, yttrium(III) nitrate was initially dissolved in the mixture of *n*-propanol and HNO_3 (solution B), before zirconium(IV) propoxide (solution A) was slowly added into it. In the case of the YSZ gels, the final molar ratio of $Zr(OC_3H_7)_4$, HNO_3, H_2O, and $Y(NO_3)_3$ were 1:2:3:0.14. Thus, the YSZ aerogel nominally contains 7 mol % yttrium.

The wet gels were transferred to perforated aluminum holders and aged during 24 h at room temperature in *n*-propanol. After this procedure, the wet gels were soaked in acetone which was replaced for fresh solvent in every 24 h for 6 days to ensure that all liquids in the gel networks are fully replaced by acetone. Our experience is that extensive and slow solvent exchange is necessary to ensure the batch-by-batch reproducibility of both the microscopic and the macroscopic structures of the final aerogels. This aging period is also necessary for secondary chemical processes to reach equilibrium before supercritical drying.

2.3. Supercritical drying (SCD)

The aged wet gels were dried in an autoclave with supercritical CO_2 by using the technique of medium temperature supercritical drying. The process is detailed in a previous publication [26]. In a typical drying procedure, the autoclave is pressurized with liquid CO_2 to 5.8 MPa, and subsequently, the temperature is raised to 80 °C, while the pressure is controlled at 18 MPa. After keeping this supercritical state for 3 h, the system is slowly depressurized to atmospheric pressure at the rate of 2 bar/min. When the autoclave is cooled down to room temperature, as-prepared monolithic ZrO_2 and YSZ aerogels are obtained.

A critical requirement for successful supercritical drying is to ensure that the as-prepared monoliths are completely free of acetone. Thus, the acetone content of CO_2 is monitored during the initial steps of the process before setting the supercritical conditions [26]. Furthermore, the IR spectra of the as-obtained aerogels should be free of –C = O resonance peaks arising from adsorbed acetone.

2.4. Heat treatment

All procedures were carried out in a standard chamber under atmospheric conditions. First, the as-prepared aerogels were kept at 300 °C for 3 h in order to remove the residual solvents. Subsequently, the aerogels were calcined at temperatures between 500 °C and 1200 °C for 2 h. The target temperature was reached with a heating rate of 10.0 °C min^{-1}. The as-obtained aerogels are denoted as follows. ZrO_2-AO and YSZ-AO: drying at 300 °C; ZrO_2-500 and YSZ-500: calcination at 500 °C; ZrO_2-1200 and YSZ-1200: calcination at 1200 °C.

2.5. Characterization techniques

Thermogravimetric analysis (TGA), differential scanning calorimetry (DSC) and coupled mass spectrometry (MS) were carried out

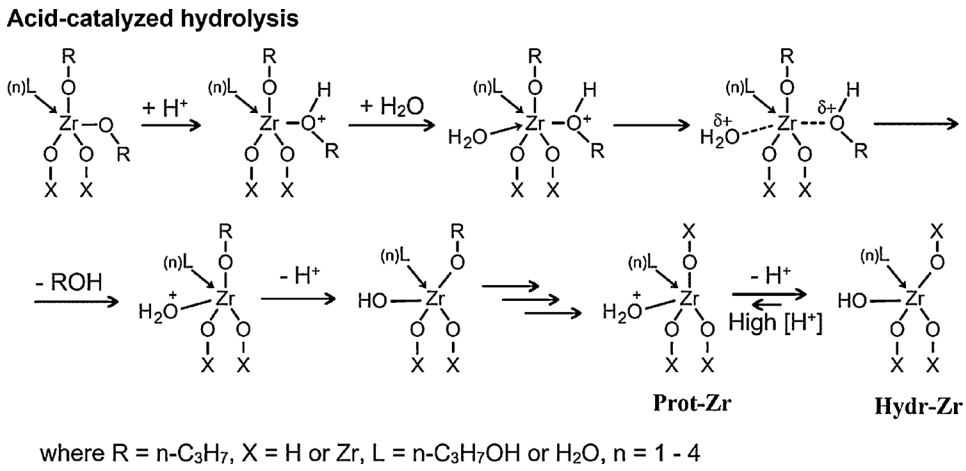

Scheme 1. The molecular mechanism of the acid-catalyzed hydrolysis of the Zr(IV) precursor leading to the formation of ZrO_2 and YSZ wet gels.

simultaneously in a Netzsch STA 409c/CD apparatus. Analyses were performed with the as-obtained aerogels ZrO_2-AO and YSZ-AO in synthetic air atmosphere (14 vol. % of O_2 in Ar) using Al_2O_3 crucibles with a heating rate of 10 °C min^{-1} from 20 °C to 1300 °C. The MS signal of *m/z*: H_2O: 18, CO: 28, CO_2: 44, NO_x: 14, 30 and 46 were recorded.

The phase recognition of the as-obtained aerogels was performed both by *in-situ* and *ex-situ* X-ray diffraction (XRD) measurements during the various stages of heat treatment. The X-Ray powder diffractometer (Empyrean; Panalytical) was set up in the Bragg-Brentano parafocusing θ – θ reflecting geometry with Cu Kα radiation (λ = 0.154 nm), Ni filter, fix divergence slits, and a 1–D position sensitive detector operated at the current of 45 mA and voltage of 40 kV. The diffraction pattern was collected from 22° to 37° with the step size of 0.0263° at the rate of 96 s per step. Total scan time was 5 min. The measurements were performed in duplicate. Data were processed using the HighScore + software and ICDD PDF 2 and ICSD 2012 databases. Quantitative phase analysis was realized according to the Rietveld method using the fundamental parameters approach. Crystallite size (*D*) was determined from the X-ray line broadening using Scherrer's equation;

$$D = K\lambda / \beta \cos\theta \quad (1)$$

where K is the shape factor (0.89), λ is the X-ray wavelength (0.154 nm), β is the line broadening at half of the maximum intensity in radians (full width at half maximum: FWHM), and θ is the Bragg angle [27]. The FWHM values were determined by fitting the XRD pattern peaks for the lattice planes $(\bar{1}11)$ and (011) for monoclinic and tetragonal, respectively. Additionally, Warren's correction was applied to the determined FWHM;

$$\beta = \sqrt{(B^2 - b^2)} \quad (2)$$

where β is the FWHM after correction, B is the calculated FWHM and b is the FWHM of the fully crystalline LaB_6 standard. When required, Rietveld refinement was performed by means of fitting the X-ray diffraction patterns using the commercially available peak fitting software HighScore+.

Nitrogen gas adsorption-desorption measurements were performed in a Quantachrome 2200e porosimeter at 77.35 K. The aerogels were degassed at 100 °C for 14 h before each measurement. The degassing temperature was chosen to be 100 °C in order to avoid any structural changes in ZrO_2-AO and YSZ-AO samples. Data were recorded and analyzed by the NovaWin 11.0 software. Surface area was calculated using the Brunauer-Emmett-Teller (BET) method from the adsorption part of the isotherm. The descriptions of the BET and *t*-plot methods, together with the definition of the *C*-constant are given in prior literature and in IUPAC technical notes [28,29]. Pore size distribution was calculated according to the Barrett-Joyner-Halenda (BJH) model from the desorption branch of the isotherm.

Scanning electron micrographs (SEM) were recorded by a Hitachi S-4300 instrument equipped with a Bruker energy dispersive X-ray spectroscope. Fresh fracture surfaces were covered by a sputtered gold conductive layer. Typically, a 5–15 kV accelerating voltage was used for taking high-resolution pictures.

3. Results and discussion

The as-obtained aerogels are denoted as follows. ZrO_2-AO and YSZ-AO were dried at 300 °C but not calcined; ZrO_2-500 and YSZ-500 were calcined at 500 °C; ZrO_2-1200 and YSZ-1200 were calcined at 1200 °C. The details of aerogel preparation are given in the Experimental section.

3.1. Mechanism of formation of ZrO_2 and YSZ wet gels

Both the ZrO_2 and YSZ aerogels were synthesized by hydrolyzing the appropriate precursors using an acidic catalyst (HNO_3). The proposed molecular mechanisms of the hydrolytic and polycondensation reactions leading to the formation of 3D gel networks are shown in Schemes 1 and 2. For the sake of visibility, the structures of octacoordinated zirconium ions are shown in a simplified form, indicating the presence of unhydrolyzed alkoxide groups, as well as bridging oxo- and/or terminal hydroxo groups.

Under acidic conditions, the first step is the protonation of an alkoxide group as shown in Scheme 1. The assumption that alkoxide group is protonated first, even in the presence of hydroxyl groups is supported by the two orders of magnitude higher protonation constant of propoxide ($\log K$ = 16.1) than that of hydroxide ($\log K$ = 14.0) [30]. Upon protonation, the partial positive charge on zirconium ion is increased, leading to a nucleophilic attack by the partially negatively charged oxygen atom of a water molecule. In a push-pull mechanism, the better leaving group ROH alcohol is split off, leaving the extra positive charge behind. Since the positive charge is located on the protonated hydroxyl group (which is the less basic group) and is repulsed by the positive charge of the zirconium ion, it is transferred to the surrounding water. Once all alkoxide groups are hydrolyzed, a completely hydrolyzed intermediate is formed (denoted as Hydr-Zr in Scheme 1). Although hydroxyl groups are somewhat weaker bases than alkoxide groups, they can be protonated in the Hydr-Zr complexes at high [H^+] concentration, resulting in an accumulation of the protonated species Prot-Zr (Scheme 1). This may be an inactive intermediate in the forthcoming condensation reactions.

A summary of the effect of acid concentration on gel formation is

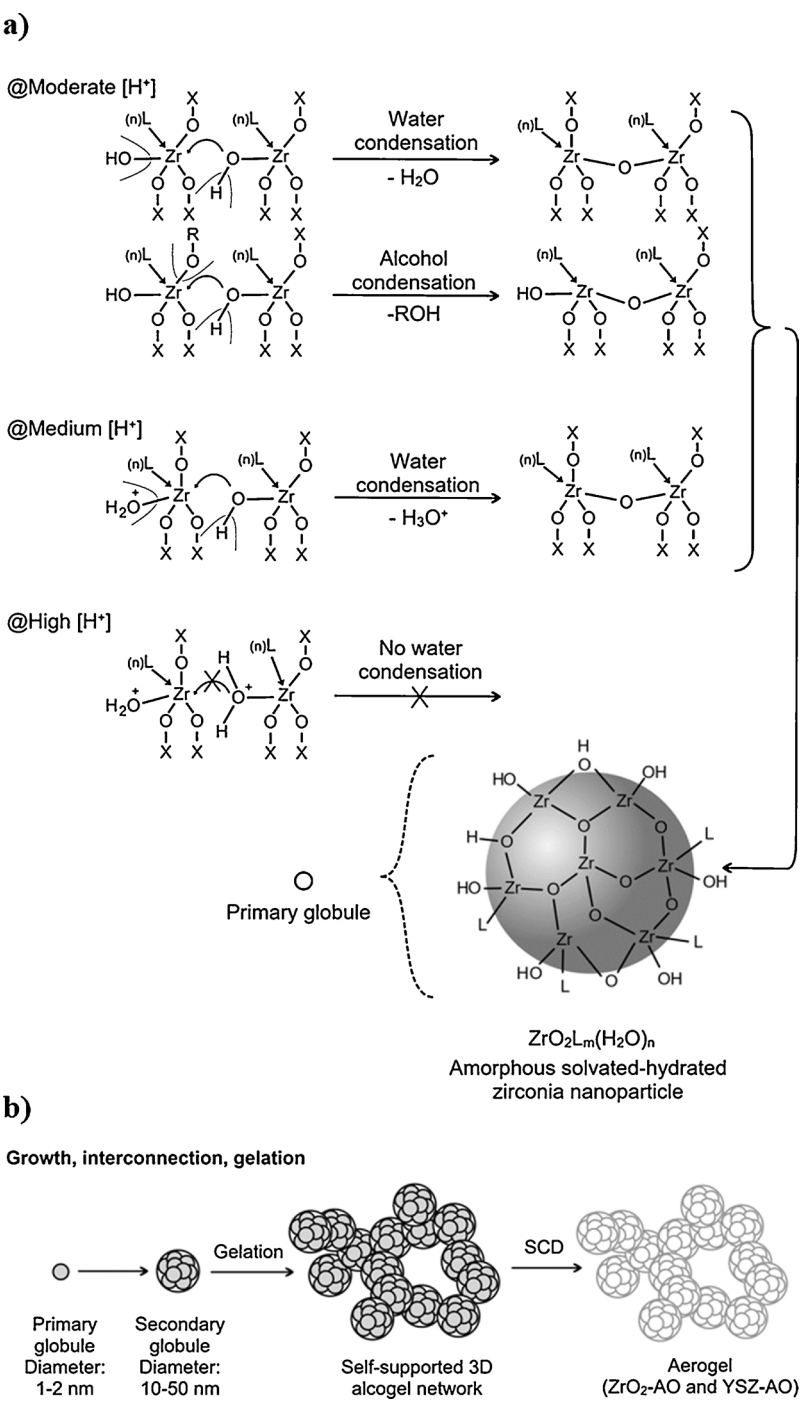

Scheme 2. a) Proposed mechanism for the formation of ZrO_2 nanoparticles and colloidal particles (sols) under different acidity conditions. b) The representation of the assembly of primary and secondary globules to a self-supported wet gel structure.

shown in Table S1, Figure S1 and Movie S1 in the Supporting Information, respectively. The rate of hydrolysis is proportional to the acid concentration in the reaction medium, and also the acid concentration has a strong impact on the rate and equilibrium state of the polycondensation reactions (Scheme 2a). Under moderately acidic conditions (@Moderate [H^+]) both water and alcohol condensation occurs simultaneously. In both cases, the nucleophilic agent is the hydroxyl group of the hydrolyzed complex Hydr-Zr, and the attack leads to the split-off of a water or alcohol molecule and the formation of bridging Zr-O-Zr bonds in the zirconia skeleton. When the acid concentration is increased (@Medium [H^+]), the protonated particles Prot-Zr are also getting involved in the water condensation process. However, under strongly acidic conditions (@High [H^+]) when most of the zirconia particles are in the protonated form, the reaction slows down very significantly (even near to stop) due to the low concentration of active Hydr-Zr species. That is why the gelation time curve shows a minimum with increasing acid concentration. The polycondensation process binds Zr atoms into a 3D ZrO_2 network, which forms tiny nanoparticles (primary globules) in the solution. In the primary globules, zirconium atoms mainly relate to each other through oxygen bridges, but other ligands like terminal or bridging OH-groups, as well as coordinated solvent and water molecules are also present. The primary globules bind to each other forming larger nanoparticles called secondary globules, which are the main building blocks of both

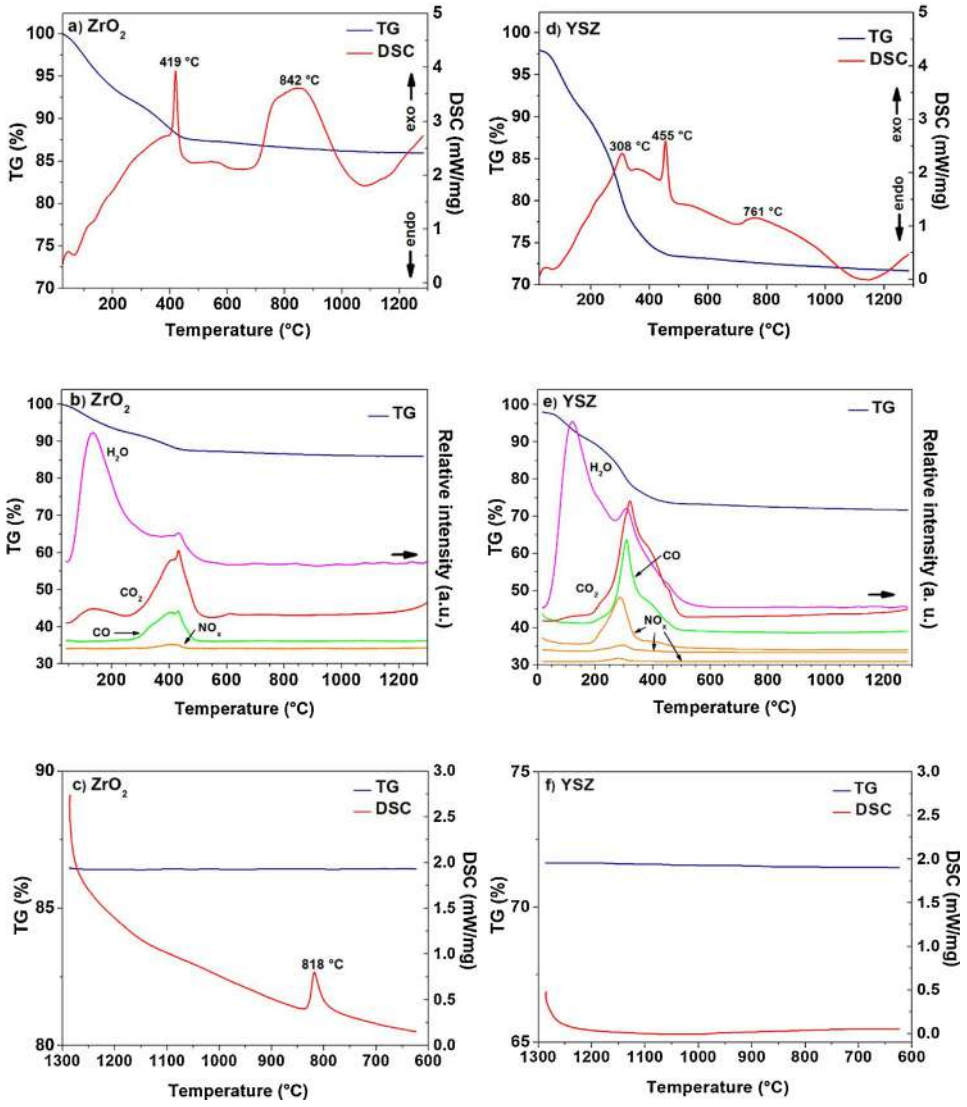

Fig. 1. Results of the thermal analysis of the as-prepared amorphous ZrO_2-AO and YSZ-AO aerogels. Comparison of the simultaneous TG/DSC signals and MS signals at *m/z*: H_2O: 18, CO: 28, CO_2: 44, and NO_x: 14; 30; 46, Graph a) and b): heating of the ZrO_2 sample. Graph c): cooling of the same sample. Graph d) and e): heating of the YSZ sample. Graph f): cooling of the same sample.

the wet gel skeleton and later the aerogel skeleton (Scheme 2b). Gelation (the formation of a self-supported wet gel) occurs when the number of secondary globules become so high that they get in contact with each other, forming an interconnected solid network. In that process, further condensation reactions occur that connect the globules with covalent chemical bonds.

When all hydrolysis and polycondensation reactions are finished, the wet ZrO_2 gel is dried under supercritical conditions with carbon dioxide. After supercritical drying, the as-obtained aerogels may contain traces of unhydrolyzed alkoxy groups, as well as solvent molecules and traces of hydrating water. Nitric acid may be present as a counter ion in the protonated structure. Residual organic moieties may serve as carbon source in high-temperature heating processes.

3.2. Thermal analysis of amorphous ZrO_2 and YSZ aerogels

The thermal analysis of the as-prepared amorphous ZrO_2-AO and YSZ-AO aerogels were performed in order to identify the presence of any energetic processes at high temperatures. The simultaneous TG and DSC results are shown in Fig. 1. These plots also show the MS signals for *m/z*: H_2O: 18, CO: 28, CO_2: 44, NO_x: 14, 30 and 46.

The first mass loss of the ZrO_2 aerogel is at 121 °C (-7.84 wt.%) and the second one is in the range of 250–400 °C (-4.87 wt.%). According to the MS data, the products that are released from the aerogel are H_2O and CO_2 in both the first and the second mass loss steps. H_2O is dominantly released at 121 °C and the release of CO_2 is characteristic at 250–400 °C. At this elevated temperature, the combustion of the left-over synthesis compounds such as *n*-propanol and HNO_3 also takes place and CO and NO_x are produced. The DSC curve shows several thermal effects. The first broad exothermic peak at 70–400 °C is consistent with the first and second mass loss steps, therefore, it is attributed to desorption and combustion processes. A sharp exothermic peak is present at 419 °C, and it is attributed to a phase transformation from amorphous to tetragonal phase (*t*-ZrO_2). There is no mass loss or MS signal at this temperature. Finally, a broad exothermic signal was detected that lies between 800 and 1100 °C with a maximum at ca. 842 °C. This signal is related to the gradual phase transition from *t*-ZrO_2 to monoclinic zirconia (*m*-ZrO_2). Both of the above discussed phase transitions were recognized by *in-situ* powder X-ray analysis as well, as described later in Section 3.6. As an additional thermal analysis step, the controlled cooling of the ZrO_2 sample was performed for identifying further thermal processes upon quenching to room temperature. The corresponding TG and DSC plots are shown in Fig. 1c. A single exothermic peak is detected at 818 °C which is related to the phase

transition from *t*-ZrO_2 to *m*-ZrO_2 (see Section 3.6).

The TG and DSC curves together with selected MS signals for the as-prepared amorphous YSZ-AO aerogel are shown in Fig. 1d-f. The TG curve shows two distinct mass loss steps at 121 °C (-7.59 wt%) and from 205 to 450 °C (-16.97 wt%). Similarly to the ZrO_2-AO sample, every mass loss step corresponds to an increase in the MS signal at *m/z* values of 18, 28, 44, 30, 14 and 46. The first mass loss step is the desorption of water at 121 °C. In the second mass loss step, residual water is removed along with combustion products such as CO_2, CO, and NO_x. The DSC curve of the amorphous YSZ aerogel sample is similar to that of the ZrO_2 sample. The first exothermic DSC peak from 70 to 400 °C is attributed to the release of heat due to combustion. The amorphous-to-tetragonal phase transition is detected at 455 °C. Interestingly, no thermal process occurs during the cooling of the YSZ sample (Fig. 1f), indicating the absence of phase transition from *t*-ZrO_2 to *m*-ZrO_2.

The measured amorphous-to-tetragonal crystallization temperatures of ZrO_2 and YSZ aerogels are 419 °C and 455 °C, respectively. The elevation of the crystallization temperature can be attributed to the presence of foreign species, such as ethoxy and nitrate groups in the YSZ aerogel [10]. This theory is supported by the significantly higher mass loss of the YSZ aerogel (-16.97 wt%) compared that of the ZrO_2 aerogel (-4.87 wt%) below 400 °C. The amount of combustion products is also much higher in the case of the YSZ sample.

3.3. Effect of calcination on the porosity of aerogels

In order to determine the effect of calcination temperature on the porosity of ZrO_2 and YSZ aerogels, N_2 adsorption-desorption isotherms were measured before and after calcination at 500 °C. The recorded N_2 adsorption-desorption curves are type IV isotherms with H1-type hysteresis loops (Fig. 2) [31]. This confirms the presence of mesopores in all aerogel samples. The structural properties of the studied aerogels are summarized in Table 1.

The ZrO_2-AO aerogel has an S_{BET} specific surface area of 255 $m^2\ g^{-1}$ and a pore volume (V_p) of 2.1 $cm^3\ g^{-1}$. As expected, due to the shrinkage of the aerogel upon calcination at 500 °C, these values decrease to 87 $m^2\ g^{-1}$ and 0.7 $cm^3\ g^{-1}$ representing a reduction of 66% and 31% for S_{BET} and V_p, respectively. On the other hand, the YSZ-AO aerogel has an S_{BET} value of 243 $m^2\ g^{-1}$ and a V_p of 1.6 $cm^3\ g^{-1}$. Heat treatment at 500 °C for 2 h resulted in a drop of S_{BET} to 113 $m^2\ g^{-1}$ (54%) but V_p did not change (1.6 $cm^3\ g^{-1}$). The measured specific surface areas are in good agreement with values published in the literature for zirconia aerogels prepared by the sol-gel method and supercritical drying [11,32–34]. Characteristic pore sizes (the peak maximum of the distribution curve) are nearly identical for the as-obtained samples, and only moderately decrease upon heating at 500 °C. Macropore volume is calculated as the cumulative pore volume of pores $d > 50$ nm. The micropore contribution to the entire surface area was calculated by using the *t*-plot method, based on the de Boer model of statistical thickness [35]. There are no pores below $d = 2$ nm in the aerogels.

The value of the *C*-constant is significantly higher for heat-treated samples, while the shape of the hysteresis loop remains unchanged. This indicates that the affinity of the probe gas (N_2) is significantly different towards the aerogel surface in AO and heat treated samples [36]. It is rational to assume that a portion of the surface is covered with residual *n*-propanol and unhydrolyzed propoxy groups in both the ZrO_2-AO and YSZ-AO aerogels. This is in agreement with the detection of combustion products at ca. 400 °C during the thermal analysis of as-prepared ZrO_2-AO and YSZ-AO samples (see Section 3.2 and Fig. 1). The heat treatment of the aerogels at 500 °C results in the desorption of residual solvents. Calcination also initiates additional alcohol condensation of the neighboring Zr-OH and Zr-OPr groups yielding new Zr-O-Zr links. The removal of residual nonpolar *n*-propanol and propoxy groups can increase the polarity of the aerogel surface, which can explain the higher values of the *C*-constant for calcined samples.

The change of the total pore volume on heating indicates the degree of shrinkage, and thus can be a good benchmark of the dimensional stability of the aerogels. As seen in Table 1, ZrO_2-AO suffers a very significant shrinkage on heating at 500 °C, indicated by the dramatic drop in pore volume from 2.1 $cm^3\ g^{-1}$ to 0.7 $cm^3\ g^{-1}$. A possible explanation is that a particle coarsening process takes place (see Section 3.4). On the other hand, YSZ-AO proved to be thermally and dimensionally more stable, because the pore volume was unchanged on heating.

3.4. Effect of calcination on surface morphology

The surface morphology and the effect of calcination temperature on the aerogel microstructure were studied by scanning electron microscopy (SEM). Fig. 3 shows the fine structure of the ZrO_2 and YSZ aerogels before and after calcination at different temperatures. The as-obtained ZrO_2-AO and YSZ-AO aerogels have similar microstructures consisting of amorphous and interconnected nanoparticle networks with no visible differences among them. After calcination at 500 °C, the morphology of both samples show a moderate restructuration. Particle sizes are a bit smaller and a small number of new macropore openings can be observed. Moreover, YSZ-500 shows viscous flow-related initial islet formation. The fine structure of YSZ-AO (Fig. 3d) is shifted to a coarser pattern after calcination at 500 °C (Fig. 3e) containing larger islets of globules. The change becomes characteristic and obvious at 1200 °C (Fig. 3f). At 1200 °C, the particles grow considerably and start to consolidate to form compact agglomerates, that is indicative of an extensive sintering process. The ZrO_2 aerogel is highly densified and the loss of almost all the porosity can be observed. Similar phenomena take place in the YSZ aerogel. Neither mesopores nor macropores are visible in the samples calcined at high temperature. An overall conclusion is that the SEM pictures are in good accordance with the porosimetry results (Fig. 2, Table 1).

3.5. Effect of calcination on crystalline structure

Ex-situ X-ray diffraction was used for the crystal structure determination of the as-obtained aerogel samples (Fig. 4). All samples were measured at room temperature after heat treatment. The pattern of the ZrO_2-AO aerogel confirms that the characteristic amorphous phase is present in the as-prepared sample after supercritical drying. Upon calcination at 500 °C for 2 h, the main diffraction peaks of monoclinic (*m*-ZrO_2, ICSD code: 18190) and tetragonal (*t*-ZrO_2, ICSD code: 72950) zirconia appear with oriented planes of ($\bar{1}$ 11), (111) and (011), (112) for monoclinic and tetragonal, respectively. In contrast with this, the calcination of the YSZ-AO sample at 500 °C yields a pure *t*-ZrO_2 phase. The calcination of the ZrO_2 aerogel at 1200 °C and cooling to room temperature induces the transition from *t*-ZrO_2 to *m*-ZrO_2 as only the *m*-ZrO_2 is present in the ZrO_2-1200 sample. Such a phase transformation is in good agreement with the exothermic peak detected during the cooling DSC curve at 818 °C (see Section 3.2 and Fig. 1c). On the other hand, the YSZ-1200 aerogel conserves the stable *t*-ZrO_2 phase after cooling to room temperature.

3.6. Crystalline phase transitions during heat treatment

The phase diagram established in 1975 by Scott shows that for pure ZrO_2, the *t*-ZrO_2 phase exists in the temperature range of 1170–2370 °C [37]. However, our findings with *ex-situ* XRD (Fig. 4) seem to have an inconsistency with this phase diagram. The as-obtained (amorphous) ZrO_2-AO aerogel partially crystallizes to *t*-ZrO_2 upon a heat treatment at 500 °C, which is far from the transformation temperature of *t*-ZrO_2 described in the phase diagram. Thus, we designed a step-by-step experiment to study the effect of temperature on the crystallographic evolution of both the ZrO_2 and the YSZ aerogels. *In-situ* XRD measurements were performed at every 100 °C during the heat treatment of

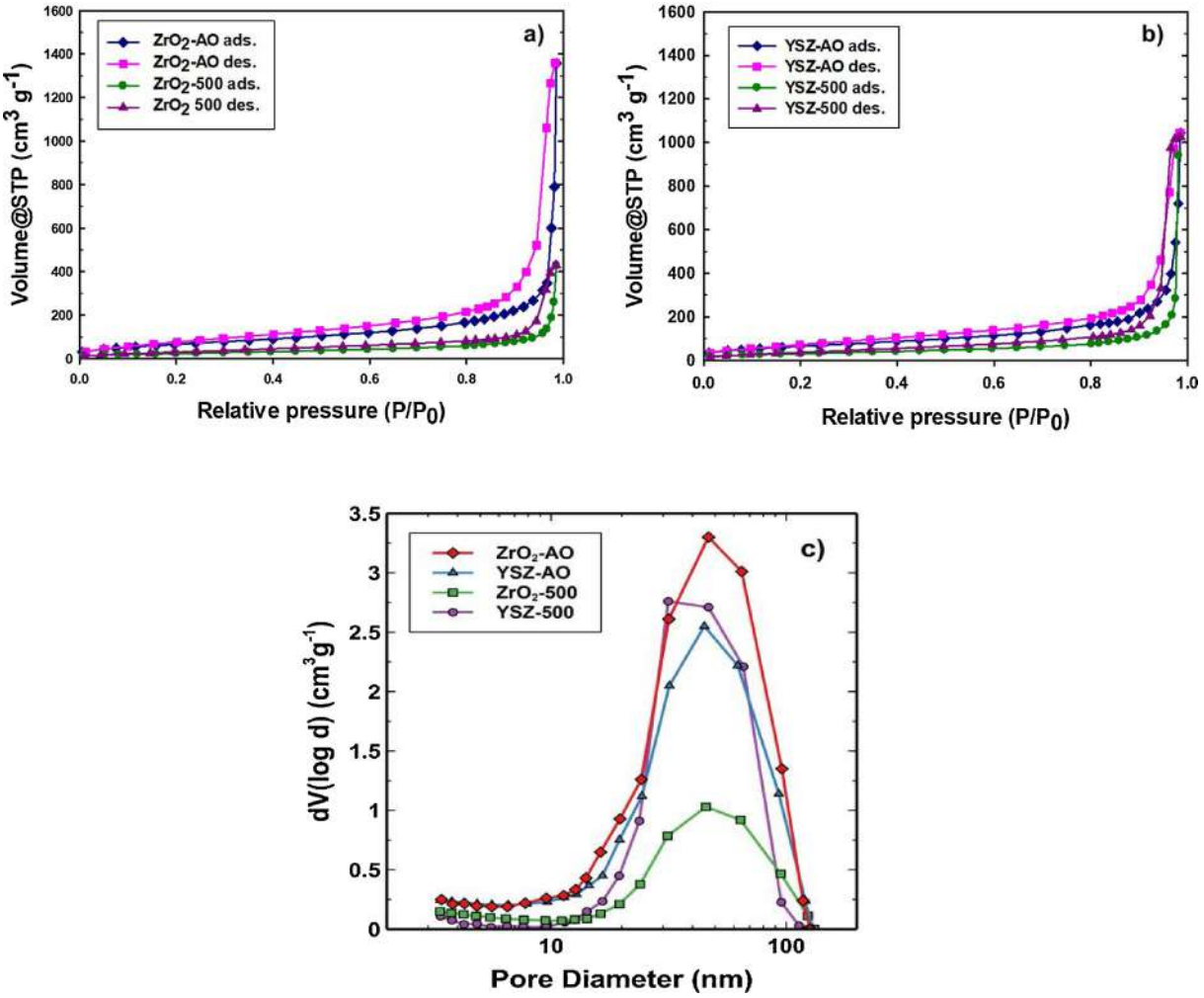

Fig. 2. Nitrogen gas adsorption (ads) – desorption (des) isotherms of ZrO_2 (a) and YSZ (b) aerogels as well as pore size distribution curves (c) before calcination (ZrO_2-AO, YSZ-AO) and after calcination at 500 °C (ZrO_2-500, YSZ-500).

the amorphous ZrO_2-AO and YSZ-AO samples up to 1200 °C. These temperature dependent XRD patterns are shown in Fig. 5. The analyses were performed from $2\theta = 22$ to 37°, because the main diffraction peaks of *m*-ZrO_2 and *t*-ZrO_2 can be clearly detected in this range.

The ZrO_2-AO sample remained unchanged up to 400 °C where only amorphous zirconia was detected. At 500 °C, partial crystallization occurs and the XRD pattern displays a diffraction peak of *t*-ZrO_2 with (011) orientation showing the formation of a dominantly tetragonal phase. New diffraction peaks appear above 700 °C corresponding to *m*-ZrO_2 with oriented planes ($\bar{1}$ 11) and (111) indicating that the tetragonal phase is transforming into a monoclinic phase. As the temperature increases to 1000 °C, the tetragonal peaks are gradually reduced, while the monoclinic peaks become more expressed. Parallel to this, the diffraction peaks become sharper with increasing calcination temperature, indicating the increase of crystallite size. At 1100 °C, most of the *m*-ZrO_2 phase is transformed to *t*-ZrO_2 marking transformation temperature from monoclinic-to-tetragonal. During the cool-down process, *t*-ZrO_2 transforms to *m*-ZrO_2, as *m*-ZrO_2 is the stable form of ZrO_2 at room temperature. In order to summarize the observations, it can be stated that pure zirconia aerogel is composed of either a single

Table 1
Textural properties of the ZrO_2 and YSZ aerogels before and after calcination. Standard deviations are displayed for primary data.

Sample	S_{BET} [m^2 g^{-1}][a]	*V*p [cm^3 g^{-1}][b]	$V_{mesopore}$ [cm^3 g^{-1}][c]	$V_{macropore}$ [cm^3 g^{-1}][d]	*D*p (nm)[e]	$D_{p\text{-}avg}$ (nm)[f]	*C*-const.[g]
ZrO_2-AO	255 ± 21	2.1 ± 0.2	1.4	0.71	47	33	39
ZrO_2-500	87 ± 13	0.7 ± 0.1	0.46	0.19	46	31	86
YSZ-AO	243 ± 14	1.6 ± 0.1	1.1	0.54	45	27	57
YSZ-500	114 ± 19	1.6 ± 0.3	1.3	0.35	37	56	83

[a] BET specific surface area.
[b] Total pore volume.
[c] Pore volume of mesopores.
[d] Pore volume of macropores.
[e] Characteristic pore diameter: estimated at the maximum of the distribution curve.
[f] Average pore size: estimated by BJH method.
[g] Constant, an indicator of the polarity of the sample surface [28,29].

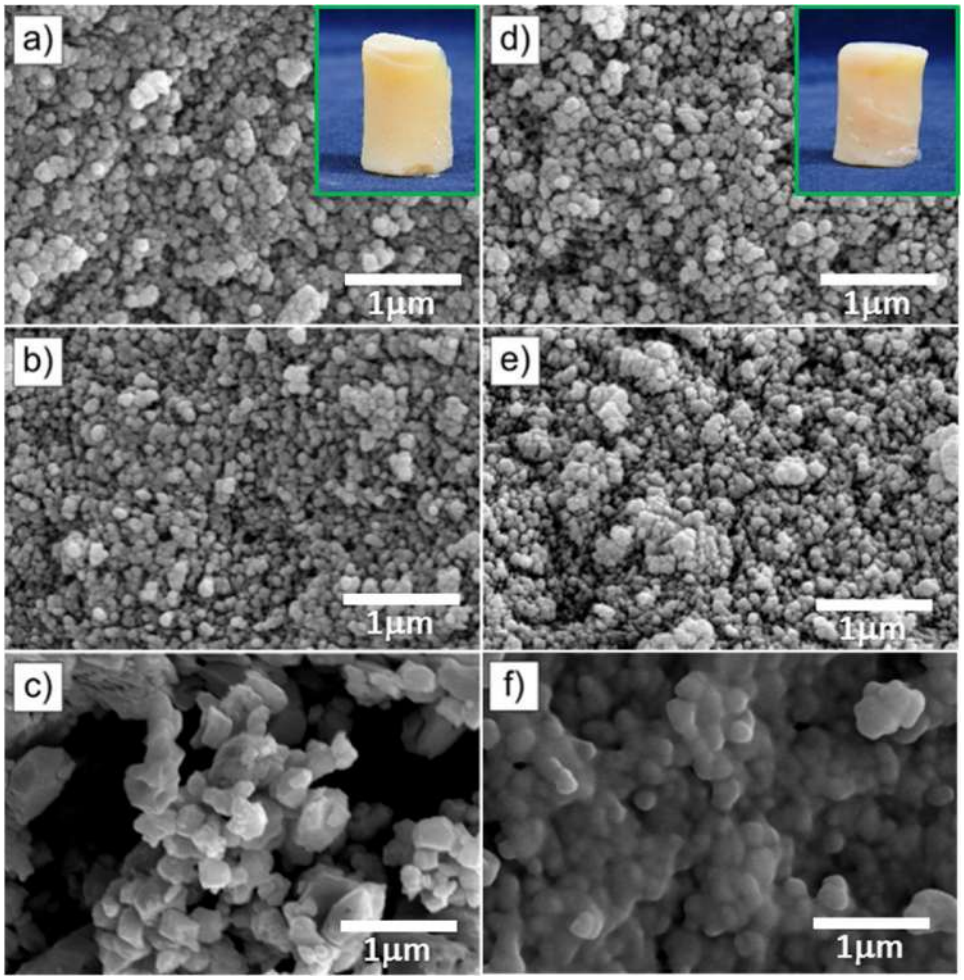

Fig. 3. SEM images of the ZrO_2 and YSZ aerogels before and after heat treatment: a) ZrO_2-AO, b) ZrO_2-500, c) ZrO_2-1200, d) YSZ-AO, e) YSZ-500 and f) YSZ-1200. Insets: photographs of the ZrO_2-AO and YSZ-AO monoliths (ca. 3 cm × 6 cm), respectively.

phase or a mixture of tetragonal and monoclinic phases between 25 and 1200 °C.

The YSZ-AO aerogel remains amorphous up to 400 °C (Fig. 5). At 500 °C, a *t*-ZrO_2 diffraction peak appears which corresponds to the crystalline plane (011). The ZrO_2 sample behaves similarly. However, in contrast to the ZrO_2 aerogel, no new diffraction peaks appear for the YSZ aerogel upon heating up to 1200 °C. Furthermore, the tetragonal phase is conserved even when the sample is cooled to room temperature. This is an obvious demonstration of the well-known stabilizing effect of yttrium ions (Y^{3+}) in the YSZ structure, promoting the formation of high purity tetragonal zirconia.

On the basis of the results of the *in-situ* XRD, the phase evolution of

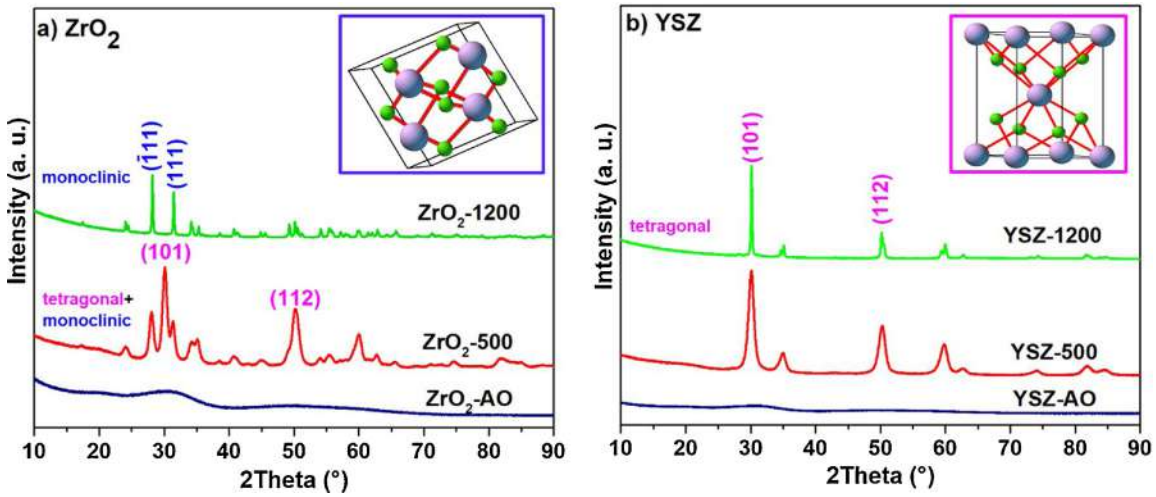

Fig. 4. X-Ray diffraction patterns of a) ZrO_2 and b) YSZ aerogels before and after calcination at 500 °C and 1200 °C for 2 h. The diffraction patterns were taken after cooling to room temperature. Insets: monoclinic (blue) and tetragonal (violet) crystalline structures of ZrO_2.

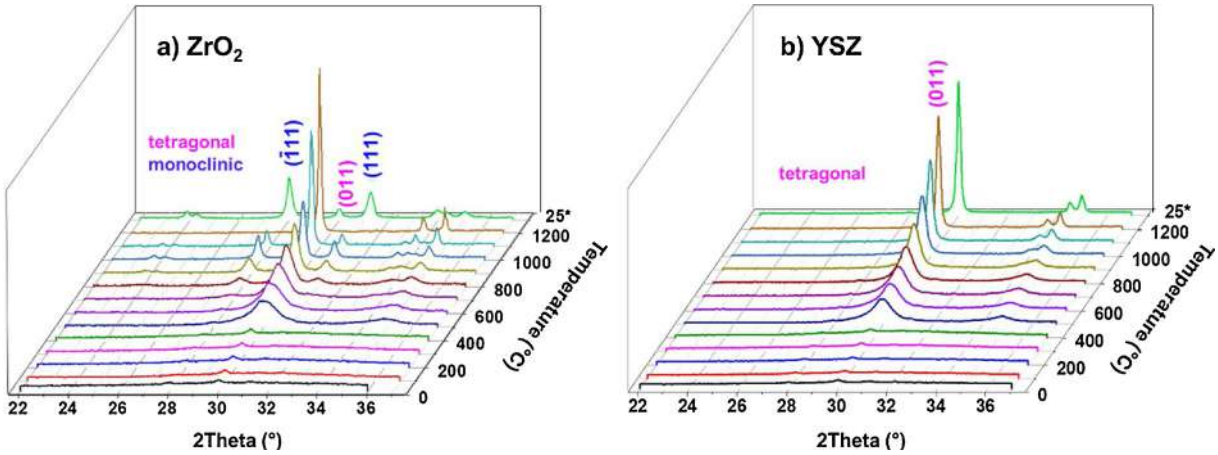

Fig. 5. Temperature dependent XRD patterns of a) ZrO_2 and b) YSZ aerogels. In-situ XRD measurements from 25 to 1200 °C were performed during the calcination of the amorphous aerogels in order to determine their crystallographic evolution. The last pattern (25*) was recorded upon quenching.

the ZrO_2 aerogel takes place during thermal treatment as follows: *i*) the initial dominantly amorphous phase transforms to a tetragonal phase at 419 °C; *ii*) in the temperature range of 500–1000 °C, a tetragonal-to-monoclinic phase transformation occurs, leading to the coexistence of a mixture of tetragonal and monoclinic phases; *iii*) the monoclinic phase is transformed to a tetragonal-dominant phase at 1100 °C with a complete transformation at 1200 °C; and *iv*) the purely tetragonal phase is transformed into a purely monoclinic phase on cooling to room temperature.

It is worth to note that the diffraction peaks are sharper at higher temperatures (Fig. 5). This indicates that the sizes of the nanometer-wide crystallites increase with increasing calcination temperature. In order to quantify the relation between phase transformation and crystallite growth, crystallite size was calculated using Scherrer's equation (Equation 1) and the crystalline phase composition of the aerogel was calculated through the Rietveld refinement. The ICSD reference patterns of *m*-ZrO_2 (ICSD code: 18190) and *t*-ZrO_2 (ICSD code: 72950) were recalculated. For the ZrO_2 aerogel, the gradual phase transformation and the crystallite size growth are shown as function of temperature in Fig. 6.

Sparsely distributed nanocrystals can exist in the amorphous matrix of the as-prepared ZrO_2-AO aerogel [38]. Such crystallites can be either monoclinic or tetragonal and can behave as preferential sites for grain growth in the dominantly amorphous ZrO_2. At 500 °C, ZrO_2 partially crystallizes to mainly *t*-ZrO_2 composed of small crystallites of ca. 6 nm

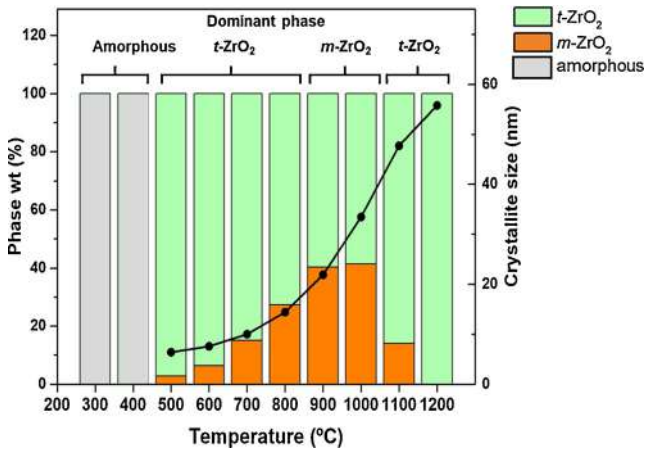

Fig. 6. The crystalline phase transitions of ZrO_2 aerogel during heat treatment. Correlation between the composition of the crystalline phase and crystallite size at different temperatures.

(Fig. 6). These nanocrystals grow within the range of 20–31 nm at 1000 °C as the amount of *t*-ZrO_2 decreases and *m*-ZrO_2 forms. With increasing temperature, *t*-ZrO_2 becomes dominant until a single-phase material is obtained at 1200 °C with a mean crystallite size of 45–52 nm.

Thus, our findings suggest that the tetragonal phase can exist in a nanometer-size domain even at lower temperatures than reported in the phase diagram of ZrO_2. Several studies have reported the existence of the tetragonal phase at room temperature and provided various explanations for such behavior. Garvie stated that the crystallite size and therefore, the free energy has an effect on the stabilization of the tetragonal crystalline phase [39]. In other words, *m*-ZrO_2 has a lower bulk free energy but *t*-ZrO_2 has a lower surface free energy. For crystallites below a certain critical size (30 nm), the surface free energy term dominates over the bulk free energy term and the stabilization of the tetragonal phase becomes favorable. Moreover, Bedilo suggested that tetragonal zirconia can exist at room temperature due the presence of organic compounds in the as-prepared aerogel matrix, as a consequence of the of sol-gel technique [17]. The burning of these organic residues during calcination leads to local overheating and the stabilization of *t*-ZrO_2. Mitsuhashi et al. reported that such stabilization is due to strain effects in the nanoparticle regime [40]. Others proposed that the formation of *t*-ZrO_2 is due to the short range structural similarities between the amorphous phase and the *t*-ZrO_2 phase [41–43]. Garvie proposed that during calcination, initially a trace amount of *m*-ZrO_2 forms, because a small portion of the crystallites are bigger than the critical phase transition size. At higher temperatures, the size of the crystallites increases and the entire sample transforms to *m*-ZrO_2.

Our experimental results clearly show that the phase transformation of ZrO_2 is complemented by crystallite size growth with increasing temperature. Furthermore, a close correlation can be identified between temperature and crystallite size in controlling the phase stability of zirconia (Figure S2) [44]. First, the amorphous ZrO_2 transforms into a *t*-ZrO_2 phase (crystallite size: 6.0–13.6 nm) in a thermodynamically controlled process that finishes at ca. 800 °C. As the temperature increases to 900 °C, the crystallite size approaches the critical size of *t*-ZrO_2 (30 nm) and the thermodynamic stability of the tetragonal and monoclinic phases become comparable. This results in a tetragonal-to-monoclinic phase transformation which becomes clearly visible at 1000 °C where the critical crystallite size is reached (31.7 nm). The temperature component becomes dominant again close to the monoclinic-to-tetragonal phase transformation temperature of 1170 °C. Subsequent heating at 1200 °C leads to the complete transformation to a pure tetragonal phase.

4. Conclusions

The acid-catalyzed sol-gel method was successfully applied to synthesize monolithic ZrO_2 and YSZ aerogels. A detailed molecular-level mechanism is proposed for the formation of the 3D wet gel network. The as-prepared monoliths were calcined at different temperatures between 300 and 1200 °C. The temperature of calcination has a marked effect on the textural properties, and the crystallinity of the aerogels. In general, the specific surface area and the total pore volume decrease on calcination regardless of the composition of the aerogels.

The YSZ sample crystallizes into a single-phase tetragonal zirconia at 455 °C and this phase is retained up to 1200 °C. Importantly, the tetragonal phase is conserved in the YSZ aerogel after cooling to room temperature. Depending on the temperature, the pure ZrO_2 aerogel can exist in either a single tetragonal phase (from 419 °C to 800 °C and over 1100 °C), or in a monoclinic phase (between 900 °C and 1000 °C), as well as in a mixture of these two phases. The evolution of the crystallinity of the ZrO_2 aerogel was studied as a function of calcination temperature by *in-situ* XRD measurements. We show that the phase transformation of ZrO_2 is complemented by crystallite size growth. Furthermore, a close correlation between temperature and crystallite size can be identified, controlling the phase stability of zirconia. An important observation is, that the mixed tetragonal and monoclinic phases are conserved when a pure ZrO_2 aerogel is calcined at 500 °C and cooled, but calcination at 1200 °C yields pure monoclinic zirconia, because a tetragonal-to-monoclinic transformation takes place on cooling to room temperature. Based on observations it is now possible to tailor physical and phase properties of zirconia aerogels for high temperature applications.

Acknowledgements

This research has been financially supported by the Ministry of Education, Youth and Sports of the Czech Republic under the project CEITEC 2020 (LQ1601). This work was supported by the ESF under the project CZ.02.2.69/0.0/0.0/18_070/0009469. Also, the authors thank the National Research, Development and Innovation Office, Hungarian Science Foundation (OTKA: FK_17-124571) for financial support. J. Kalmár was supported by the ÚNKP-17-4 NEW NATIONAL EXCELLENCE PROGRAM of the Ministry of Human Capacities, Hungary. The research was supported by the EU and co-financed by the European Regional Development Fund under the projects GINOP-2.3.2-15-2016-00008 and GINOP-2.3.2-15-2016-00041 projects. Part of the work was carried out with the support of CEITEC Nano Research Infrastructure (MEYS CR, 2016–2019).

Appendix A. Supplementary data

Supplementary material related to this article can be found, in the online version, at doi:https://doi.org/10.1016/j.supflu.2019.02.011.

References

[1] S.S. Kistler, Coherent expanded-aerogels, J. Phys. Chem. 36 (1931) 52–64.
[2] K. Maghsoudi, S. Motahari, Mechanical, thermal, and hydrophobic properties of silica aerogel-epoxy composites, J. Appl. Polym. Sci. 135 (2018) 45706.
[3] S. Iswar, W.J. Malfait, S. Balog, F. Winnefeld, M. Lattuada, M.M. Koebel, Effect of aging on silica aerogel properties, Microporous Mesoporous Mater. 241 (2017) 293–302.
[4] L.W. Hrubesh, Aerogel applications, J. Non-Cryst Solids 225 (1998) 335–342.
[5] I. Smirnova, P. Gurikov, Aerogel production: current status, research directions, and future opportunities, J. Supercrit. Fluid 134 (2018) 228–233.
[6] C. Ziegler, S. Klosz, L. Borchardt, M. Oschatz, S. Kaskel, M. Friedrich, R. Kriegel, T. Keilhauer, M. Armbruster, A. Eychmuller, ZnPd/ZnO aerogels as potential catalytic materials, Adv. Funct. Mater. 26 (2016) 1014–1020.
[7] J.F. Liu, N.W. Liu, K.Q. Ren, L. Shi, X. Meng, Sulfated zirconia synthesized in a one step solvent-free method for removal of olefins from aromatics, Ind. Eng. Chem. Res. 56 (2017) 7693–7699.
[8] C.C. Wei, K. Li, Yttria-stabilized zirconia (YSZ)-based hollow fiber solid oxide fuel cells, Ind. Eng. Chem. Res. 47 (2008) 1506–1512.
[9] P. Khajavi, A.A. Babaluo, A. Tavakoli, A. Mirzaei, Stabilization of the metastable tetragonal phase in zirconia nanopowders synthesized via polyacrylamide gel method, Ind. Eng. Chem. Res. 53 (2014) 164–172.
[10] C. Stocker, A. Baiker, Zirconia aerogels: effect of acid-to-alkoxide ratio, alcoholic solvent and supercritical drying method on structural properties, J. Non-Cryst Solids 223 (1998) 165–178.
[11] N. Shimoda, K. Nakayama, K. Kiyota, S. Satokawa, Synthesis of tetragonal zirconia in mesoporous silica and its catalytic properties for methanol oxidative decomposition, RSC Adv. 7 (2017) 55819–55829.
[12] B. Tyagi, K. Sidhpuria, B. Shaik, R.V. Jasra, Synthesis of nanocrystalline zirconia using sol−gel and precipitation techniques, Ind. Eng. Chem. Res. 45 (2006) 8643–8650.
[13] J. Fenech, C. Viazzi, J.P. Bonino, F. Ansart, A. Barnabe, Morphology and structure of YSZ powders: comparison between xerogel and aerogel, Ceram. Int. 35 (2009) 3427–3433.
[14] D.J. Suh, T.J. Park, Sol−gel strategies for pore size control of high-surface-area transition-metal oxide aerogels, Chem. Mater. 8 (1996) 509–513.
[15] D.J. Suh, T.J. Park, H.Y. Han, J.C. Lim, Synthesis of high-surface-area zirconia aerogels with a well-developed mesoporous texture using CO2 supercritical drying, Chem. Mater. 14 (2002) 1452–1454.
[16] A. Benad, F. Jurries, B. Vetter, B. Klemmed, R. Hubner, C. Leyens, A. Eychmuller, Mechanical properties of metal oxide aerogels, Chem. Mater. 30 (2018) 145–152.
[17] A.F. Bedilo, K.J. Klabunde, Synthesis of high surface area zirconia aerogels using high temperature supercritical drying, Nanostruct. Mater. 8 (1997) 119–135.
[18] T. Gotsch, W. Wallisch, M. Stoger-Pollach, B. Klotzer, S. Penner, From zirconia to yttria: Sampling the YSZ phase diagram using sputter-deposited thin films, AIP Adv. 6 (2016) 025119.
[19] C.N. Chervin, B.J. Clapsaddle, H.W. Chiu, A.E. Gash, J.H. Satcher, S.M. Kauzlarich, Aerogel synthesis of yttria-stabilized zirconia by a non-alkoxide sol−gel route, Chem. Mater. 17 (2005) 3345–3351.
[20] Z. Zhao, D. Chen, X. Jiao, Zirconia aerogels with high surface area derived from sols prepared by electrolyzing zirconium oxychloride solution: comparison of aerogels prepared by freeze-drying and supercritical CO2(l) extraction, J. Phys. Chem. C 111 (2007) 18738–18743.
[21] J.B. Miller, S.E. Rankin, E.I. Ko, Strategies in controlling the homogeneity of zirconia silica aerogels - effect of preparation on textural and catalytic properties, J. Catal. 148 (1994) 673–682.
[22] Z.G. Wu, Y.X. Zhao, D.S. Liu, The synthesis and characterization of mesoporous silica–zirconia aerogels, Microporous Mesoporous Mater. 68 (2004) 127–132.
[23] G.Q. Zu, J. Shen, L.P. Zou, W.B. Zou, D.Y. Guan, Y. Wu, Y.W. Zhang, Highly thermally stable zirconia/silica composite aerogels prepared by supercritical deposition, Microporous Mesoporous Mater. 238 (2017) 90–96.
[24] Q. Sun, Y.L. Zhang, J.F. Deng, S.Y. Chen, D. Wu, A novel preparation process for thermally stable ultrafine tetragonal zirconia aerogel, Appl. Catal. A 152 (1997) L165–L171.
[25] C. Brinker, G. Scherer, Sol-Gel Science, London (1990).
[26] I. Lázár, I. Fábián, A continuous extraction and pumpless supercritical CO2 drying system for laboratory-scale aerogel production, Gels 2 (2016) 26.
[27] F.T. Muniz, M.A. Miranda, C. Morilla Dos Santos, J.M. Sasaki, The Scherrer equation and the dynamical theory of X-ray diffraction, Acta Crystallogr. A 72 (2016) 385–390.
[28] K. Sing, The use of nitrogen adsorption for the characterisation of porous materials, Colloid Surf. A 187 (2001) 3–9.
[29] M. Thommes, K. Kaneko, A.V. Neimark, J.P. Olivier, F. Rodriguez-Reinoso, J. Rouquerol, K.S.W. Sing, Physisorption of gases, with special reference to the evaluation of surface area and pore size distribution (IUPAC Technical Report), Pure Appl. Chem. 87 (2015) 1051–1069.
[30] IUPAC, Stability Constants Database: Mini-SCDatabase Software, Stability Constants Database: Mini-SC Database Software, (2018) (Accessed: June-2018), http://www.acadsoft.co.uk.
[31] K.S.W. Sing, S.J. Gregg, Adsorption, Surface Area and Porosity, New York (1982).
[32] H. Gao, Z. Zhang, Z. Shi, J. Zhang, M. Zhi, Z. Hong, Synthesis of high-temperature resistant monolithic zirconia-based aerogel via facile water glass assisted sol–gel method, J. Solgel Sci. Technol. 85 (2018) 567–573.
[33] Z. Shi, H. Gao, X. Wang, C. Li, W. Wang, Z. Hong, M. Zhi, One-step synthesis of monolithic micro-nano yttria stabilized ZrO_2 -Al_2O_3 composite aerogel, Microporous Mesoporous Mater. 259 (2018) 26–32.
[34] Z.Y. Zhang, Q.Y. Gao, Y. Liu, C.M. Zhou, M.J. Zhi, Z.L. Hong, F. Zhang, B. Liu, A facile citric acid assisted sol-gel method for preparing monolithic yttria-stabilized zirconia aerogel, RSC Adv. 5 (2015) 84280–84283.
[35] C.J. Gommes, A.P. Roberts, Stochastic analysis of capillary condensation in disordered mesopores, Phys. Chem. Chem. Phys. 20 (2018) 13646–13659.
[36] D. Dollimore, P. Spooner, A. Turner, The bet method of analysis of gas adsorption data and its relevance to the calculation of surface areas, Surf. Technol. 4 (1976) 121–160.
[37] H.G. Scott, Phase relationships in the zirconia-yttria system, J. Mater. Sci. 10 (1975) 1527–1535.
[38] D.A. Ward, E.I. Ko, Synthesis and structural transformation of zirconia aerogels, Chem. Mater. 5 (1993) 956–969.
[39] R.C. Garvie, The occurrence of metastable tetragonal zirconia as a crystallite size effect, J. Phys. Chem. 69 (1965) 1238–1243.
[40] T. Mitsuhashi, M. Ichihara, U. Tatsuke, Characterization and stabilization of metastable tetragonal ZrO_2, J. Am. Ceram. Soc. 57 (1974) 97–101.
[41] V.G. Keramidas, W.B. White, Raman scattering study of the crystallization and phase transformations of ZrO_2, J. Am. Chem. Soc. 57 (1974) 22–24.
[42] J. Li Vage, K. Doi, C. Mazieres, Nature and thermal evolution of amorphous hvdrated zirconium oxide, J. Am. Chem. Soc. 51 (1968) 349–353.
[43] E. Tani, M. Yoshimura, S. Somiya, Formation of ultrafine tetragonal ZrO_2 powder under hydrothermal conditions, J. Am. Ceram. Soc. 66 (1983) 11–14.
[44] X.X. Xu, X. Wang, Fine tuning of the sizes and phases of ZrO2 nanocrystals, Nano Res. 2 (2009) 891–902.